Spectroscopic and Computational Studies on the Coordination-Driven Self-Assembly Complexes $(ZnL)_2$ and $(NiL)_2$ [L= Bis(2,4-dimethyldipyrrin-3-yl)methane]

Wei Li,[†,‡] Yi-Bo Wang,[§] Lan-Ying Yang,[||] Xu-Feng Shan,[||] Xuan Cai,[†] Adriana Szeghalmi,[⊥] Yong Ye,[†] Jin-Shi Ma,[||] Ming-Dao Luo,[†] Jiming Hu,*[,†] and Wolfgang Kiefer[⊥]

College of Chemistry and Molecular Sciences, Wuhan University, Wuhan 430072, China, Department of Chemical Engineering, Wuhan University of Science and Engineering, Wuhan 430073, China, Department of Chemistry, Guizhou University, Guiyang, Guizhou 550025, China, Key Laboratory of Photochemistry, Institute of Chemistry, Chinese Academy of Sciences, Beijing 100080, China, and Institut für Physikalische Chemie, Universität Würzburg, Am Hubland, D-97074 Würzburg, Germany

Received: May 21, 2006; In Final Form: August 12, 2006

FT-IR, FT-Raman and electronic absorption spectroscopies were utilized in conjunction with density functional theory (DFT) calculations to investigate the ground and excited states of self-assembled dinuclear dimeric helicates $(ZnL)_2$ and $(NiL)_2$ [L = bis(2,4-dimethyldipyrrin-3-yl)methane]. These studies afford a detailed description of the ground-state geometric and electronic structures of $(ZnL)_2$ and $(NiL)_2$ and provide a comparison with similar geometrical metal−porphyrins. The results demonstrate that enlarging the basis set used in the DFT calculations results in an obvious alteration of the calculated bond lengths but negligible alteration of the calculated bond angles. The predicted spectra are in good agreement with the experimental ones with the deviations generally less than 30 cm^{-1}. In comparison with vibrational spectra of metal−porphyrins, the breathing vibration of the pyrrole ring is shifted by over 100 cm^{-1} toward higher wavenumber due to local conjugation of molecular geometry. Time-dependent density functional theory (TD-DFT) provides a good description of the excitation energy. Because of the break in symmetry, the absorption band (corresponding to the Q-band of porphyrin) of $(ZnL)_2$ and $(NiL)_2$ is no longer weak. Local conjugation makes the absorption wavelength of $(NiL)_2$ and $(ZnL)_2$ shift to the blue compared with those of NiP and ZnP.

Introduction

Coordination-driven self-assembly plays a crucial role in supramolecular chemistry.[1−7] Among many ligands designed by chemists, polybipyridine ligands developed by Lehn and his colleagues are particularly interesting with respect to their ability to generate helicates,[8] grids,[9] cages,[10] ladders,[11] and rings.[12] In contrast to bipyridine, dipyrrin (**I**; Figure 1) was recently found to be an ideal building block for supramolecular self-assembly.[13−16] Dipyrrin, formerly called dipyrromethene, is a yellow, fully conjugated, flat molecule containing 10π electrons. It is the important building block for porphyrins, bile pigments, and linear polypyrroles.[17−20] In dipyrrin, the hydrogen at the N−H group can be removed, and the resulting monoanionic species is a resonance-stabilized ligand. The complexes generated by **I** and metal ions are neutral species, therefore, counterions are not needed. Consequently, the complexes are particularly convenient for purification by column chromatography since they are not charged and are generally the least polar component in the reaction mixtures. Self-assembly of bis(dipyrrins) such as biladiene-ac (**II**),[13−16] 3,3′-bidipyrrins (**III**),[17,18] and bis(dipyrrin-3-yl)methane (**IV**) has been reported. Interestingly, by varying the bridge spacers between two dipyrrin units, the self-assembly of the corresponding bis(dipyrrin) ligands with metal ions, such as Zn(II), gives supramolecules with different geometric shapes. For example, the Zn(II) complexes of ligands **II** and **IV** are dinuclear dimeric helicate,[13−16] while that of ligand **III** is a trinuclear trimeric triangle.[17,18] More recently, the dynamics of self-assembly, such as the structural control of the excited-state dynamics of bis(dipyrrinato) zinc complex, and excited-state energy-transfer dynamics in self-assembled triads composed of two porphyrins and an intervening bis(dipyrrinato)-metal complex have been reported.[21,22] Furthermore, the energy transfer followed by electron transfer in a supramolecular triad composed of boron dipyrrin and zinc porphyrin was also studied.[23]

It is exceedingly difficult to develop accurate force fields for molecules of the size and complexity of $(ZnL)_2$ and $(NiL)_2$ [L = bis(2,4-dimethyldipyrrin-3-yl)methane] on a purely empirical basis. Quantum mechanical calculations of force constants can solve the difficulties of empirical force field determination by making available independent information, which is largely complementary to the spectroscopic measurements.[24] As an economical and effective way of including electron correlation in the ground-state wavefunction, gradient-corrected density functional theory (DFT) is about as inexpensive as Hartree−Fock theory and is much more accurate for molecules composed of first-row atoms. Wong[25,26] has shown that the Becke−Lee−Yang three-parameter hybrid functional (B3LYP) yields remarkably accurate vibrational wavenumbers. For the size of $(NiL)_2$ and $(ZnL)_2$, the 6-31G(d) basis set appears to be a reasonable compromise between cost and accuracy. Recently, the time-dependent density functional theory (TD-DFT) with exact exchange has been quite successful in predicting the electronic spectra of porphin,[27] tetraphenylporphyrin, and its β-octahalo-

* To whom correspondence should be addressed. Fax: +86-027-68754067. E-mail: jmhu@whu.edu.cn.
† Wuhan Univeristy.
‡ Wuhan University of Science and Engineering.
§ Guizhou University.
|| Chinese Academy of Sciences.
⊥ Universität Würzburg.

10.1021/jp063105i CCC: $33.50
Published on Web 10/07/2006

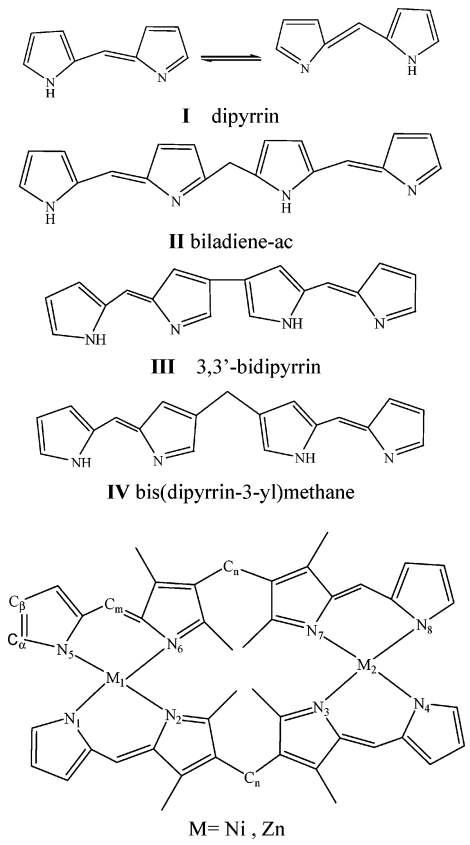

Figure 1. 1. Structures of dipyrrin, dimmer, and $(NiL)_2$ and $(ZnL)_2$.

genated derivatives.[28] In the present study, the FT-Raman and -IR spectra of $(ZnL)_2$ and $(NiL)_2$ were measured, and their ground-state geometries, electronic structures, and vibrational spectra were calculated by DFT/B3LYP with various basis set combinations and compared with those of zinc(II) and nickel-(II) porphyrins, which have geometrical similarity.

Experimental and Computational Methods

(1) Syntheses and Sample Preparation. $(NiL)_2$ and $(ZnL)_2$ were synthesized by the following procedure.

$(NiL)_2$. A solution of 2,2′4,4′-tetramethyl-3,3′-dipyrromethane-5,5′-dicarboxylic acid (0.25 mmol) in 2 mL of trifluoroacetic acid was stirred at room temperature for 10 min. Then, a solution of pyrrole-2-carbaldehyde (0.5 mmol) in 5 mL of methanol was added, followed by 1 mL of HBr−HOAC (45%). After the mixture was stirred for 2 h, 0.1 g of nickel acetate and 1 g of sodium acetate in methanol (20 mL) were added to the solution and stirring was continued for 1 h. The reaction mixture was poured into 40 mL of H_2O and extracted with $CHCl_3$ (30 mL $\times$ 3). The $CHCl_3$ extract was evaporated under vacuum, and the residue was purified with silica gel chromatography using CH_2Cl_2 as eluent to give the complex $(NiL)_2$. Red crystals of $(NiL)_2$ for X-ray analysis were obtained by recrystallization from $CHCl_3/CH_3OH$. Yield: 60%. Anal. Calcd for $C_{46}H_{44}N_8Ni_2$: C, 66.86; H, 5.37; N, 13.56. Found: C, 67.03; H, 5.48; N, 13.44. MALDI-TOF-MS: $m/z = 825$ $[M^+ + H]$

$(ZnL)_2$. This compound was prepared similarly to $(NiL)_2$ with the modification that nickel acetate was replaced by zinc acetate dihydrate. Red crystals suitable for X-ray analysis were obtained by recrystallization in CH_2Cl_2, Yield: 65%. Anal. Calcd for $C_{46}H_{44}N_8Zn_2$ (CH_2Cl_2): C, 61.06; H, 5.02; N, 12.12. Found: C, 60.85; H, 4.88; N, 11.91.

(2) Spectroscopy. Samples were dissolved in dichloromethane. A Perkin-Elmer UV−vis−near-IR spectrometer (model Lambda 19) was used to record the UV−vis absorption spectra. The FT-Raman spectra were recorded in the solid state with an IFS 120HR spectrometer equipped with an integrated FRA 106 (Bruker) Raman module. The 1064 nm radiation from a Nd:YAG laser was used for excitation. Laser powers of 100 and 150 mW were selected for $(ZnL)_2$ and $(NiL)_2$, respectively. A high-sensitivity Ge detector was used, and each spectrum represented 1000 scans. The spectral resolution was 4 cm^{-1}, and the region of interest was 150−3600 cm^{-1}. The FT-IR spectra were measured with a model 170SX FT-IR spectrometer (Nicolet) in KBr tablets, and the spectral range was 400−4000 cm^{-1}.

(3) Calculations. Becke's [29a−d] 1988 exchange functional in combination with Becke's three-parameter hybrid exchange functional using the LYP[29e] correlation functional of Lee, Yang, and Parr (B3LYP) was employed in the DFT calculations. To understand the influence of the basis set on optimized geometries, the following basis sets were used for the geometry optimization of $(NiL)_2$: standard 6-31G(d) split valence basis set for all atoms (designated as basis set 1); LANL2DZ effective core potential (ECP) basis set for the nickel atom and 6-31G-(d) basis set for all other atoms (designated as basis set 2); the 6-31+G (d) basis set for all atoms (designated as basis set 3). For $(NiL)_2$, analytical frequency calculation was done by B3LYP with basis set 2 for the optimized geometry obtained from the basis set 2 calculation. For $(ZnL)_2$, basis set 1 was used for the geometry optimization and the analytical frequency calculation. The assignment of the calculated wavenumbers was aided by the animation option of HyperChem[30] and GaussView graphical interface for GAUSSIAN programs, which gives a visual presentation of the structure of the vibrational modes. The HyperChem vibrational spectrum with active IR vector rendering has been used to graphically display the normal modes associated with individual vibrations.

The excitation energy and oscillator strength calculations were carried out using time-dependent density functional response theory[31] as implemented in the Gaussian98 program.[32] The TD-DFT calculations, carried out with the basis set 2 optimized structures, were done at the B3LYP/6-31G(d) level of theory. For comparison, semiempirical calculations with ZINDO/S [33] were carried out using Hyperchem software. The excitations with energy of less than 9 eV were considered, and 1.267 $\sigma-\sigma$ and 0.50 $\pi-\pi$ overlap weighting factors were used for the ZINDO/S calculations. The theoretical spectra were simulated with the GaussSum 4.01 program.[34] The line shape was of Lorentzian type, and the fwhm (full width at half-maximum) was 5 cm^{-1}. The spectral range was 50−1800 cm^{-1} for Raman and 400−1800 cm^{-1} for FT-IR.

Results and Discussion

(1) Molecular Structures. Figure 1 gives the structures of $(ZnL)_2$ and $(NiL)_2$. They are formed by coordination of two metal ions and two bis(2,4-dimethyldipyrrin-3-yl)methane ligands. A single-crystal X-ray diffraction (XRD) experiment revealed that both of them have double stranded helical geometry. The selected optimized geometrical parameters of $(ZnL)_2$ and $(NiL)_2$ along with their single-crystal XRD data are included in Table 1. Due to the different sizes of the central metal cations in $(ZnL)_2$ and $(NiL)_2$, the spatial structure of the complexes presents some difference. The bond length of Zn−N is longer by 0.014−0.035 Å than that of Ni−N, and the bond angle of N−M−N (M = Ni and Zn) changes from 2 to 16°.

TABLE 1: Selected Bond Lengths and Bond Angles of $(NiL)_2$ and $(ZnL)_2$ Calculated at Different Levels of Theory[a]

$(NiL)_2$					$(ZnL)_2$		
	B3LYP/ basis set 1	B3LYP/ basis set 2	B3LYP/ basis set 3	single-crystal XRD		B3LYP/ basis set 1	single-crystal XRD
			bond length (Å)				
Ni(1)−N(1)	1.900	1.924	1.922	1.937(4)	Zn(1)−N(1)	1.990	1.962(4)
Ni(1)−N(2)	1.909	1.933	1.929	1.966(4)	Zn(1)−N(2)	2.010	2.005(4)
Ni(1)−N(5)	1.900	1.924	1.922	1.949(4)	Zn(1)−N(5)	1.990	1.971(5)
Ni(1)−N(6)	1.909	1.933	1.929	1.964(4)	Zn(1)−N(6)	2.000	1.986(4)
Ni(2)−N(3)	1.915	1.941	1.938	1.975(4)	Zn(2)−N(3)	2.000	1.986(4)
Ni(2)−N(4)	1.899	1.924	1.920	1.954(4)	Zn(2)−N(4)	1.980	1.971(5)
Ni(2)−N(7)	1.915	1.941	1.938	1.969(4)	Zn(2)−N(7)	2.010	2.005(4)
Ni(2)−N(8)	1.899	1.924	1.920	1.950(4)	Zn(2)−N(8)	1.980	1.962(4)
Ni(1)−Ni(2)	8.822	8.862	8.840	8.122	Zn(1)−Zn(2)	8.421	8.083
C_n−C_n	6.700	6.730	6.751	7.626	C_n−C_n	7.510	7.744
			bond angle (deg)				
N(1)−Ni(1)−N(5)	126.8	127.6	127.4	125.70(1 7)	N(1)−Zn(1)−N(5)	118.6	119.00(18)
N(1)−Ni(1)−N(6)	96.4	96.5	96.7	116.04(1 7)	N(1)−Zn(1)−N(6)	124.7	122.55(17)
N(5)−Ni(1)−N(6)	93.6	93.1	93.1	93.53(17)	N(5)−Zn(1)−N(6)	96.3	95.89(18)
N(1)−Ni(1)−N(2)	93.6	93.0	93.1	92.49(16)	N(1)−Zn(1)−N(2)	96.3	95.85(16)
N(5)−Ni(1)−N(2)	126.8	127.7	127.4	124.20(1 6)	N(5)−Zn(1)−N(2)	124.7	118.27(17)
N(6)−Ni(1)−N(2)	95.2	95.1	95.2	104.78(1 5)	N(6)−Zn(1)−N(2)	108.8	106.25(16)
N(8)−Ni(2)−N(4)	126.9	127.9	127.8	133.15(1 7)	N(8)−Zn(2)−N(4)	119.0	122.55(17)
N(8)−Ni(2)−N(7)	93.7	93.2	93.3	93.51(17)	N(7)−Zn(2)−N(8)	96.6	95.85(16)
N(4)−Ni(2)−N(7)	126.9	127.9	127.6	118.14(1 6)	N(4)−Zn(2)−N(7)	119.0	119.00(18)
N(8)−Ni(2)−N(3)	95.4	95.2	96.1	112.40(1 7)	N(8)−Zn(2)−N(3)	109.9	106.25(16)
N(4)−Ni(2)−N(3)	93.7	93.3	93.3	94.38(16)	N(3)−Zn(2)−N(4)	96.6	95.89(18)
N(7)−Ni(2)−N(3)	95.9	95.9	95.1	102.61(1 5)	N(3)−Zn(2)−N(7)	118.7	118.27(17)

[a] Basis set 1: 6-31G(d) for all atoms. Basis set 2: 6-31G(d) for N, C, H; lanl2dz for Ni. Basis set 3: 6-31+G(d) for all atoms.

For $(ZnL)_2$, the predicted structure is in good agreement with the experimental structure to a degree which is typical for this level of theory applied to a large conjugated system. Specifically, the predicted bond lengths are longer by about 0.02 Å than the experimental values. The differences in bond angle are within 2° with the exception of N(5)−Zn(1)−N(2), which is larger by 6.5° than the experimental value. Single-crystal XRD results show that the distances of Zn−Zn and C_n–C_n are 8.083 and 7.744 Å, respectively. The bond distances of Zn(1)−Zn(2) and C_n–C_n calculated at the B3LYP/6-31G(d) level of theory are 8.421 and 7.510 Å, respectively. The DFT calculation presents a slightly flatter and longer geometry than the experimental one.

A significant difference appears between the calculated and observed geometries of $(NiL)_2$.The predicted bond lengths are generally shorter than the experimental ones by 0.015−0.035 Å, and the differences in bond angle are 0.4−3.5°, except for N(1)−Ni(1)−N(6), N(6)−Ni(1)−N(2), and N(4)−Ni(2)−N(7), which deviate significantly from the XRD results. The differences are 20.0, 9.6, and 9.8°, respectively. An enlarged basis set increases the bond length by 0.02−0.03 Å but exerts a very slight influence on bond angles. The optimized geometry obtained from basis set 2 calculations is closer to the XRD experimental structure than the ones obtained from basis sets 1 and 3. Consequently, the structure from basis set 2 was used as the geometry for analytical frequency calculation. XRD revealed that the distances of Ni−N and C_n–C_n of $(NiL)_2$ are 8.122 and 7.626 Å, respectively. The predicted Ni−Ni distance is longer by about 0.7 Å, but C_n–C_n is shorter by about 0.9 Å than the actual distance. The distances of Ni−Ni and C_n–C_n calculated at various levels of theory reveal small differences. An enlarged basis set makes the distances of Ni−Ni and C_n–C_n increase slightly.

(2) Ground-State Electronic Structure. The orbital energy levels of $(NiL)_2$ and $(ZnL)_2$ calculated at various levels of theory, are summarized in Table 2. The Mulliken population analysis reveals that the highest four occupied orbitals of $(ZnL)_2$ receive the same characteristic contribution from C_α and C_β atoms and have mainly π-bonded orbital character. Accordingly, the neighboring four frontier orbital energy levels are very close but not degenerate. Taking $(ZnL)_2$ for example, the energy levels of HOMO, HOMO-1, HOMO-2, and HOMO-3 are −5.012, −5.046, −5.142, and −5.225 eV, respectively. The gaps between neighboring orbitals are 0.034, 0.096, and 0.083 eV, respectively. The HOMO-4 coefficients are largely localized on the pyrrole nitrogen and C_β atoms. So, the energy level of HOMO-4 is significantly lower than those of the four highest occupied MOs. Similarly, the energy levels of the four lowest unoccupied MOs are close to each other and significantly lower than that of LUMO-4. A similar phenomenon occurs in $(NiL)_2$. The only difference appears on HOMO-4. DFT calculations show that HOMO-4 of $(NiL)_2$ receives a major contribution from the d_{xy} orbital of nickel ion.

TABLE 2: Frontier Orbital Energy Levels of $(NiL)_2$ and $(ZnL)_2$ (eV)[a]

	$(NiL)_2$			$(ZnL)_2$
orbita	B3LYP/ basis set 1	B3LYP/ basis set 2	B3LYP/ basis set 3	B3LYP/ basis set 1
LUMO+4	−1.431(*dxy*)	−1.747(*dxy*)	−1.982(*dxy*)	1.198(π*)
LUMO+3	−1.877(π*)	−1.906(π*)	−2.201(π*)	−1.887(π*)
LUMO+2	−1.997(π*)	−2.032(π*)	−2.338(π*)	−1.922(π*)
LUMO+1	−2.033(π*)	−2.084(π*)	−2.344(π*)	−1.994(π*)
LUMO	−2.156(π*)	−2.188(π*)	−2.457(π*)	−2.055(π*)
HOMO	−5.025(π)	−5.052(π)	−5.300(π)	−5.012(π)
HOMO-1	−5.061(π)	−5.080(π)	−5.342(π)	−5.046(π)
HOMO-2	−5.167(π)	−5.195(π)	−5.441(π)	−5.142(π)
HOMO-3	−5.190(π)	−5.213(π)	−5.482(π)	−5.225(π)
HOMO-4	−5.386(*dyz*)	−5.595(*dyz*)	−5.825(*dyz*)	−5.967(π)

[a] Basis set 1: 6-31G(d) for all atoms. Basis set 2: 6-31G(d) for N, C, H; lanl2dz for Ni. Basis set 3: 6-31+G(d) for all atoms.

The orbital energy levels of $(ZnL)_2$ calculated at the same level of theory are close to those of $(NiL)_2$. With an enlarged basis set, the orbital energy level for $(NiL)_2$ is lowered. The orbital energy levels obtained by using basis set 2 are close to

TABLE 3: Calculated Wavenumber, Raman Activity, IR Intensity, and Observed Fundamentals of $(NiL)_2$[a]

	calc			obs			
assignment	wavenumber[b] (cm^{-1})	IR intensity[c]	Raman activity	IR	Raman	NiP [36]	NiOEP [36]
$\upsilon(C_\beta-H)$	3097.4	40.0	187.7	3105			
$\upsilon(C_\beta-H)$	3079.9	5.7	62.9	3087			
$\upsilon(C_\beta-H)$	3036.8	16.4	7.7	3027			
$\upsilon_{asym}(CH_3)$	2967.8	68.5	10.1	2952			
$\upsilon_{sym}(CH_3)$	2897.4	105.0	25.2	2904			
$\upsilon_{sym}(CH_2)$	2886.4	52.6	34.6	2850			
$\upsilon(C_\alpha-C_m)_{asym}$	1609.7	147.8	174.1		1603	1611	1603
$\upsilon(C_\alpha-C_m)_{asym}$	1604.3	2403.8	10.6	1601		[1624][d]	
$\upsilon(C_\beta-C_\beta)$	1526.7	16.3	232.7		1565	1574	1577
$\upsilon(C_\beta-C_\beta)$	1502.2	105.1	11.9	1500		1505	
$\delta_{as}(CH_3)$	1447.4	0.9	41.6		1449		
$\delta_{as}(CH_3)$	1440.9	211.1	19.1	1435			
υ(pyr half-ring)$_{sym}$	1397.1	13.3	166.0		1390	1376	1383
υ(pyr half-ring)$_{sym}$	1395.8	286.8	4.1	1388			
υ(pyr quarter-ring)	1368.6	77.9	0.7	1362		1368	[1396]
υ(pyr quarter-ring)	1371.7	0.9	163.2		1358	1354	1393
υ(pyr quarter-ring)	1279.6	1282.4	1.5	1270			
υ(pyr quarter-ring)	1273.5	35.2	250.6		1274		
$\delta(C_\alpha-H)+\delta(C_\beta-H)_{asym}$	1163.7	0.2	68.5		1173	1185	
$\delta(C_\alpha-H)+\delta(C_\beta-H)_{asym}$	1175.7	197.4	0.0	1172			
$\upsilon_{as}(C_\beta-C_{n-}C_\beta)$	1133.5	108.9	0.9	1155			
υ(pyr breathing)	1105.0	28.8	0.8	1102		1003	804
υ(pyr breathing)	1099.5	99.7	1.3	1095		[995]	[751]
υ(pyr breathing)	1081.8	0.7	103.8		1092	995	766
$\delta(C_\beta-H)_{sym}$	1041.9	0.1	12.3		1036	1066	
$\delta(C_\beta-H)_{sym}$	1044.9	510.5	0.0	1032		[1064]	
CH_3 rock	969.5	698.9	0.5	987			
$\delta(C_\alpha-H)+\delta(C_\beta-H)$	983.5	0.9	126.8		983		
CH_3 rock	920.5	14.8	0.1	920			
CH_3 rock	923.3	2.5	1.0		920		
$\delta(C_m-H)$	898.0	15.4	0.2	903			
CH_3 rock	888.5	66.4	0.1	883			
CH_3 rock	886.6	0.2	16.9		888		
δ(pyr def)$_{asym}$	861.2	20.7	8.6	852		819	938
δ(pyr def)$_{asym}$	860.7	0.0	13.4		850		
δ(pyr def)$_{asym}$	786.7	149.5	36.0	793		[806]	
δ(pyr def)$_{asym}$	785.1	111.5	57.5		791	806	[927]
$\gamma(C_\beta-H)+\gamma(C_\alpha-H)$	734.1	0.2	3.4		745		
$\gamma(C_\beta-H)+\gamma(C_\alpha-H)$	733.6	96.8	0.0	743			
δ(pyr def)$_{sym}$	678.5	84.5	1.7	690		732	746
δ(pyr def)$_{sym}$	674.8	0.4	6.8		693	[745]	
out-of-plane def of pyr	657.6	5.8	0.0	676			
out-of-plane def of pyr	637.6	0.1	38.6		654		
out-of-plane def of pyr	634.9	15.8	0.0	653			
out-of-plane def of pyr	582.9	7.5	0.5	597			
δ(pyr rot.)	552.2	11.2	4.2	566			551
δ(pyr def)$_{sym}$	549.7	2.3	23.3		552		
δ(pyr rot.)	535.2	20.7	0.7	516		435	493
$\delta(C_\alpha-CH_3)$	449.0	14.6	0.1	457			
υ(Ni−N)	410.3	0.0	21.3		419	420	
υ(Ni−N)	431.4	17.8	0.0	415			
υ(Ni−N)	340.0	0.0	21.7		328	369	360
υ(Ni−N)	249.4	1.7	17.1		258	237	168
δ(pyr transl)	207.0	0.1	12.6		202	197	
δ(pyr transl)	134.9	0.1	12.1		125		

[a] Abbreviations and symbols: asym, asymmetric; sym, symmetric; pyr, pyrrole; def, deformation; rot., rotation; transl, translation; υ, stretch; δ, bending; γ, out-of-plane wagging. [b] Scaled by 0.9614 with the exception of υ(C−H); 0.95. [c] IR intensity: KM $(mol)^{-1}$. [d] Values in square brackets are from IR spectra.

the ones obtained by using basis set 1, but significantly higher than the ones obtained by using basis set 3.

(3) Vibrational and Electronic Spectra. The vibrational wavenumbers and IR and Raman intensities of $(ZnL)_2$ and $(NiL)_2$ were determined by B3LYP with basis set 1 or basis set 2 at the optimized geometry. It is known that ab initio and DFT potentials systematically overestimate the vibrational wavenumbers. These discrepancies can be corrected by directly scaling the calculated values with a proper factor.[35] In the present work, all calculated harmonic wavenumbers were scaled by a common (for this level of theory) factor of 0.9614,[35] excepting the ν(C−H) modes. Due to the more anharmonic character of this mode, a smaller scaling factor of 0.95 had to be used for its adjustment. According to the calculated wavenumbers and their intensities, the normal-mode analysis, and the literature, the experimental fundamentals are then assigned (Tables 3 and 4). Also, the resonance Raman and FT-IR spectra of NiP,[36a] NiOEP,[36b] and ZnP [37] are present in Tables 3 and 4.

Both $(ZnL)_2$ and $(NiL)_2$ have 294 vibrational modes. The absence of imaginary wavenumbers confirms that the local minima on the potential energy surface have been found. Comparing the scaled wavenumbers with the experimental

TABLE 4: Calculated Wavenumber, Raman Activity, IR Intensity, and Observed Fundamentals of $(ZnL)_2$[a]

	calc			obs		
assignment	wavenumber[b] (cm^{-1})	IR intensity	Raman activity[c]	IR	Raman	ZnP [37]
$\upsilon(C_\beta-H)$	3101.4	34.2	591.6	3102		
$\upsilon(C_\beta-H)$	3080.0	20.2	167.0	3084		
$\upsilon(C_\beta-H)$	3028.5	16.4	6.4	3027		
$\upsilon_{asym}(CH_3)$	2966.6	44.2	25.2	2949		
$\upsilon_{asym}(CH_2)$	2917.9	39.5	14.3	2922		
$\upsilon_{sym}(CH_2)$	2886.8	68.0	6.1	2853		
$\upsilon(C_\alpha-C_m)$	1599.6	527.1	158.6		1603	1607
$\upsilon(C_\alpha-C_m)$	1591.4	1860.5	49.8	1601		
$\upsilon(C_\beta-C_\beta)$	1538.1	41.1	88.5		1567	1558
$\upsilon(C_\beta-C_\beta)$	1501.3	42.8	10.5	1500		1517
$\delta_{as}(CH_3)$	1467.3	0.0	44.7		1456	
$\delta_{as}(CH_3)$	1467.2	80.3	6.0	1455		
$\delta_{as}(CH_3)$	1441.6	71.0	8.6	1435		
υ(pyr half-ring)	1387.5	332.5	13.3	1388		[1385][d]
υ(pyr half-ring)	1388.9	1.5	176.5		1386	1384
υ(pyr quarter-ring)	1353.3	103.6	3.1	1363		[1347]
υ(pyr quarter-ring)	1281.7	405.7	62.4		1274	1299
υ(pyr quarter-ring)	1279.	873.4	41.3	1273		
$\delta(C_\alpha-H)+\delta(C_\beta-H)_{asy\ m}$	1172.1	115.5	10.0	1180		
$\delta(C_\alpha-H)+\delta(C_\beta-H)_{asy\ m}$	1172.7	52.5	12.9		1179	
$\upsilon_{as}(C_\beta-C_{n-}C_\beta)$	1169.9	39.3	31.2		1162	
$\upsilon_{as}(C_\beta-C_{n-}C_\beta)$	1135.8	151.8	1.8	1158		
$\upsilon_{as}(C_\beta-C_{n-}C_\beta)$	1126.6	1.0	6.7		1146	
υ(pyr breathing)	1102.5	57.9	0.9	1105		997
υ(pyr breathing)	1095.8	133.6	2.2	1091		
υ(pyr breathing)	1074.3	0.1	126.6		1088	
$\delta(C_\beta-H)_{sym}$	1044.4	484.1		1037		1052
$\delta(C_\beta-H)_{sym}$	1039.5	4.9	35.1		1032	1019
$\delta(C_\alpha-H)+\delta(C_\beta-H)$	980.8	20.7	21.3	981	983	993
CH_3 rock	914.0	36.1	1.1	922	917	
CH_3 rock	877.8	54.7	2.1	886		
CH_3 rock	875.7	5.5	10.5		889	
δ(pyr def)$_{asym}$	864.2	7.7	14.3		854	
δ(pyr def)$_{asym}$	864.1	11.3	6.2	850		849
δ(pyr def)$_{asym}$	781.7	144.1	37.4	799	787	799
$\gamma(C_\beta-H)+\gamma(C_\alpha-H)$	739.0	40.2	0.4	749		739
δ(pyr def)$_{sym}$	690.9	1.1	19.3		693	
δ(pyr def)$_{sym}$	680.8	88.1	0.9	693		699
out-of-plane def of pyr	667.5	23.1	1.8	676		
out-of-plane def of pyr	641.9	0.3	15.0		658	
out-of-plane def of pyr	585.6	8.5	0.2	600		
out-of-plane def of pyr	555.0	0.0	22.4		549	
δ(pyr rot.)	520.5	12.0	4.8	513		
$\delta(C_\alpha-CH_3)$	443.9	17.5	0.2	457		
υ(Zn−N)	384.8	0.2	36.8		426	
υ(Zn−N)	324.7	1.5	20.5		332	367
υ(Zn−N)	265.0	2.8	20.4		265	
υ(Zn−N)	233.5	3.2	8.7		237	
δ(pyr transl)	202.7	0.0	2.9		213	
δ(pyr transl)	126.4	0.1	7.9		118	

[a] Abbreviation and symbols: asym, asymmetric; sym, symmetric; pyr, pyrrole; def, deformation; rot., rotation; υ, stretch; δ, bending; γ, out-of-plane wagging. [b] Scaled by 0.9614 with the exception of υ(C−H); 0.95. [c] Raman activity in $Å^4$ $(amu)^{-1}$. [d] Values in square brackets are from IR spectra.

fundamentals, we see that the deviations are typically less than 30 cm^{-1} (except for a few cases when the deviations are out of this range).

The FT-Raman and FT-IR spectra of $(NiL)_2$ and $(ZnL)_2$ are present in Figures 2and 3. For comparison, the simulated spectra and experimental ones are also shown in Figure 4. As seen from Figures 2 and 3, the FT-Raman and IR spectra of $(NiL)_2$ and $(ZnL)_2$ reveal similarities in most of the band patterns. Small differences appear in the position and relative intensity of some bands. Those bands above 1800 cm^{-1} in FT-Raman spectra are too weak to be observed, so we only present the spectra in the range of 50−1800 cm^{-1}. In FT-IR spectra, all bands in the full range of 400−3500 cm^{-1} were observed. We note that the bands at 2334−2337 and 2361 cm^{-1} are the characteristic bands of CO_2 gas.

The normal-mode analysis and the experimental spectra show that the characteristic skeletal vibrational modes of the pyrrole ring are present in FT-Raman and -IR spectra of $(NiL)_2$ and $(ZnL)_2$ as well as in spectra of NiP, NiOEP, and ZnP. As for the same vibrational mode, the shift in wavenumber is within 30 cm^{-1} with the exception of a few modes.

Comparing the calculated wavenumber scaled by the factor of 0.9614 with the observed fundmental, the DFT calculations underestimate significantly the vibrational wavenumber of mode $\upsilon(C_\beta-C_\beta)$ and υ(Zn−N). For $\upsilon(C_\beta-C_\beta)$, the calculated values are 1526.7 cm^{-1} for $(NiL)_2$ and 1538.1 cm^{-1} for $(ZnL)_2$, while the observed fundamentals are 1565 and 1567 cm^{-1} for $(NiL)_2$ and $(ZnL)_2$, respectively. The calculation underestimates the wavenumbers by about 39 and 29 cm^{-1}, respectively. In the same way, the calculated wavenumber of the Zn−N stretching

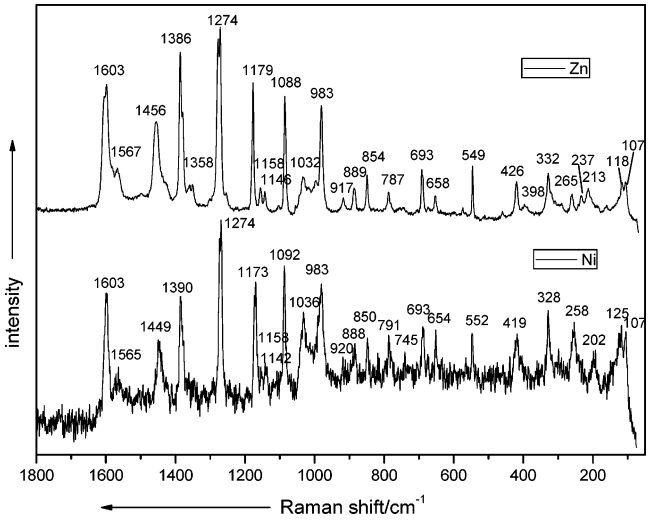

Figure 2. 2. FT-Raman spectra of $(ZnL)_2$ and $(NiL)_2$.

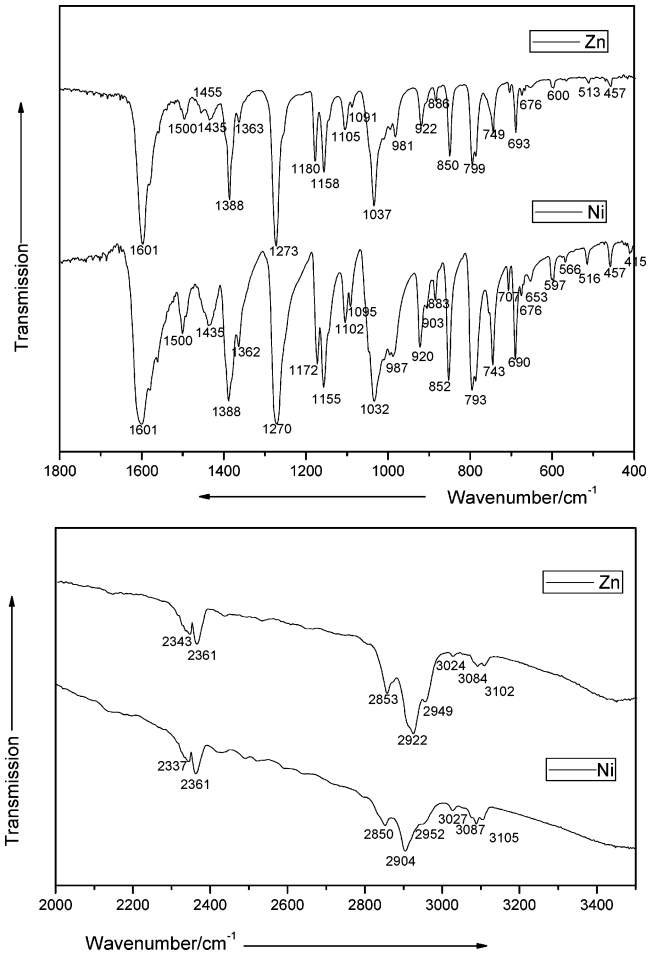

Figure 3. 3. FT-IR spectra of $(NiL)_2$ and $(ZnL)_2$.

vibration is 384.8 cm^{-1}, but the observed one is 426 cm^{-1}.The difference is about 42 cm^{-1}. For the other modes, the calculation reproduces well the experimental spectra.

Besides the vibrational band of pyrrole ring and bridging methene, the insertion of a metal ion in the center of the molecule results in new vibrational modes. The Ni−N stretching vibrations can be observed at 415 cm^{-1} in the IR spectrum and at 419, 328, and 258 cm^{-1} in the Raman spectrum. Analogously, the Zn−N stretching vibrations appear at 426, 332, 265, and 237 cm^{-1} in the Raman spectrum.

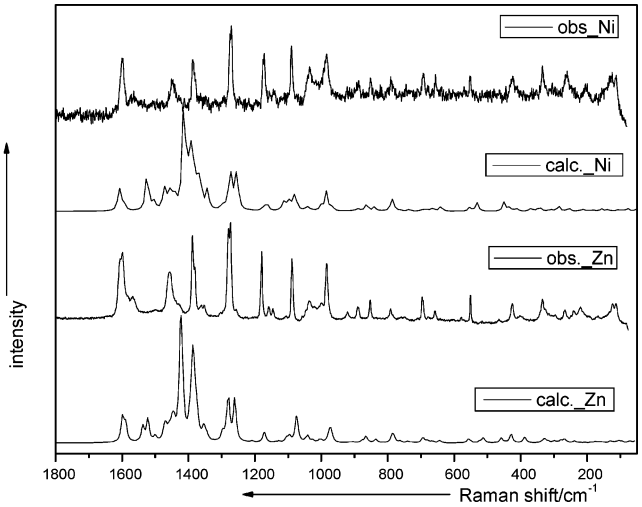

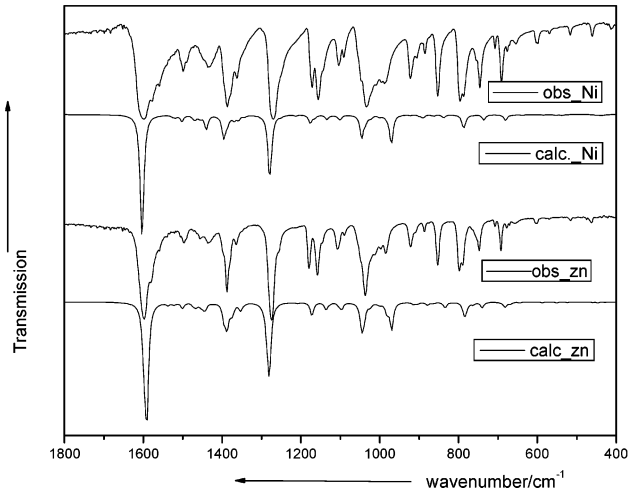

Figure 4. 4. Comparison of vibrational spectra between simulation and experiment.

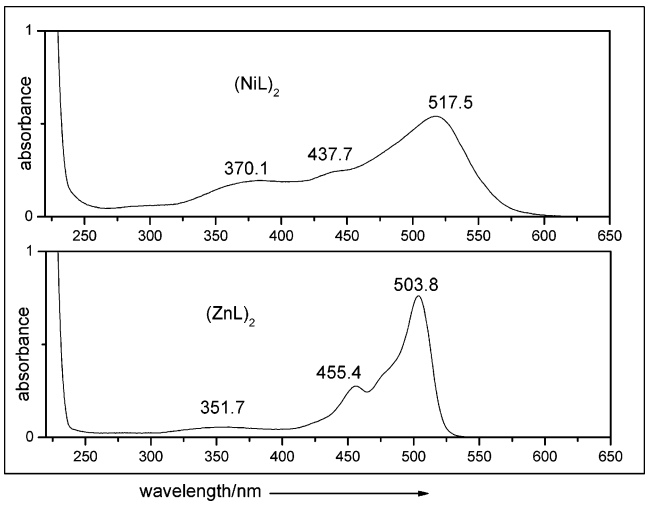

Figure 5. 5. UV−vis absorption spectra of $(NiL)_2$ and $(ZnL)_2$.

Comparing the vibrational spectra of $(ZnL)_2$ and $(NiL)_2$ with those of the NiP, NiOEP, and ZnP, a significant difference appears on the breathing vibration mode of the pyrrole ring. For $(ZnL)_2$ and $(NiL)_2$, the breathing vibrations of the pyrrole ring appears at 1102−1105 and 1091−1095 cm^{-1}, respectively, in the IR spectrum and at 1088−1092 cm^{-1} in the Raman spectrum. However, the same mode had been observed at 1003, 995 cm^{-1} (NiP), 804 cm^{-1} (NiOEP), and 997 cm^{-1} (ZnP). The

TABLE 5: Excitation Energies (eV) and Oscillator Strength (*f*) Obtained from TDDFT-B3LYP/6-31G(d) and ZINDO/S

expt(eV/nm)	excited states	composition	excitation energy (eV)	wavelength (nm)	oscillator strength	assignment	ZINDO/S	NiP[a]
$(NiL)_2$								
2.40 (517.5)	10^1A	H−0→L+0(+65%) H−1→L+2(12%) H−2→L+1(+7%) H−0→L+4(+6%)	2.44	508.3	0.0569	$\pi\rightarrow\pi^*$	2.51 (0.0001)	2.28 (Q)
2.83 (437.7)	14^1A	H−1→L+2(+31%) H−2→L+0(22%) H−0→L+1(+17%) H−2→L+1(10%) H−0→L+0(+5%)	2.66	466.7	0.0964	$\pi\rightarrow\pi^*$	2.84 (3.8293)	Sh_1
3.35 (370.1)	18^1A	H−3→L+1(+25%) H−1→L+3(18%) H−0→L+2(+17%) H−2→L+0(15%) H−1→L+1(+8%)	3.18	389.9	0.0011	$\pi\rightarrow\pi^*$	3.20 (0.0648)	3.11 (B)
$(ZnL)_2$								ZnP
2.46 (503.8)	1^1A	H−0→L+0(+44%) H−1→L+1(22%) H−1→L+3(+12%) H−0→L+2(+8%)	2.58	479.9	0.0020	$\pi\rightarrow\pi^*$	2.74 (2.9913)	2.21,[b] 2.23,[c] 2.18[d] (Q)
2.73 (455.4)	9^1A	H−2→L+2(+54%) H−1→L+2(+12%) H−2→L+0(+9%) H−0→L+3(7%) H−3→L+1(7%) H−3→L+3(+6%)	2.82	440.1	0.0770	$\pi\rightarrow\pi^*$	2.97 (2.0239)	Sh_1
3.53 (351.7)	14^1A	H−2→L+2(+17%) H−3→L+3(+14%) H−3→L+1(+14%) H−0→L+3(+7%) H−2→L+0(6%)	3.14	395.3	1.3782	$\pi\rightarrow\pi^*$	3.13 (0.0418)	3.09,[b] 3.18,[c] 3.13[d] (B)

[a] CS_2 solution spectrum of NiP, ref 38. [b] Data taken in C_6H_6, ref 39. [c] Data taken in *n*-octane, ref 40. [d] Data taken in MeOH, ref 41.

difference is larger than 100 cm^{-1}. What causes this large discrepancy? We consider that it may arise for the following reason. The double stranded helical conformation of $(NiL)_2$ and $(ZnL)_2$ is a local conjugation system, while in NP, NiOEP, and ZnP, the macrocyclic planar geometry, is a full conjugation system. The full electronic conjugation averages significantly the bond order of single and double bonds. Consequently, the wavenumber of the pyrrole ring breathing vibration is shifted toward lower wavenumber. For $(ZnL)_2$ and $(NiL)_2$, the local conjugation limits the influence on the average of the bond order. As a result, the breathing vibration of the pyrrole ring appears at a higher wavenumber.

$(NiL)_2$ and $(ZnL)_2$ have some similarity in the UV−vis absorption spectra (in Figure 5). 18 singlet excited states of $(NiL)_2$ and $(ZnL)_2$ were calculated by TD-DFT. For comparison, the energies of the Q and B bands of NiP and ZnP are also gathered in Table 5. First, we consider $(NiL)_2$ from the TD-DFT model; the strong and broad band of $(NiL)_2$ centered at 2.40 eV is assigned to the 10^1A excited state, which is described by a major contribution of the H−0→L+0(+65%) transition. The computed TD-DFT overestimates the excitation energies in dichloromethane by 0.04 eV. A weak shoulder band, which can be found on the high-energy side of this strong band and located at 2.66 eV, is described by a 'minus' combination of the H−1→L+2(+31%), H−2→L+0(22%), H−0→L+1(+17%), and H−2→L+1(10%) configurations. TD-DFT underestimates its excitation energy by 0.17 eV. Another broad band located at 3.35 eV is assigned to the 18^1A state [H−3→L+1(+25%), H−1→L+3(18%), H−0→L+2(+17%), and H−2→L+0(15%)]. The excitation energy of 3.18 eV obtained from the TD-DFT calculation is slightly lower (0.17 eV) than the experimental value obtained in dichloromethane. We note that all the transitions discussed above are of $\pi\rightarrow\pi^*$ types.

In the discussion above, we have discussed the UV−vis spectrum of $(NiL)_2$. We now turn our attention to the spectrum of $(ZnL)_2$. The strong band centered at 2.46 eV is assigned to the 1^1A state and is described by a minus combination of H−0→L+0(+44%) and H−1→L+1(22%) configurations. The computed excitation energy (2.58 eV) is slightly higher than the experimental value. A shoulder band located at 2.73 eV is assigned to the 9^1A state, which mainly originates from the H−2→L+2(+54%) excitation. A weak broad band can be found at 3.53 eV. TD-DFT calculation reveals that it can be assigned to the 14^1A state, which is described by the combination of H−2→L+2(+17%), H−3→L+3(+14%), and H−3→L+1-(+14%) configurations. The computed TD-DFT underestimates the excitation energy by 0.39 eV. The excitation energy and oscillator strength of $(ZnL)_2$ and $(NiL)_2$ were also computed by ZINDO/S. In general, the TD-DFT calculation provides a more reliable result than ZINDO/S.

The origin and the intensities of the lowest absorptions of metal−porphyrins, the Q and B bands, were successfully explained by Gouterman's four-orbital model. According to the four-orbital model, the B and Q bands can be described in terms of transition between a pair of top filled orbitals (a_{1u} and a_{2u}) and lowest empty orbitals (the doubly degenerate e_g). The near degeneracy of the $a_{1u}{}^1e_g{}^1$ and $a_{2u}{}^1e_g{}^1$ excited configurations leads to a strong configuration interaction that results in a high-lying state corresponding to the B band and a low-lying state corresponding to the Q band. The configuration mixing combines the transition dipoles of the individual one-electron transition in such a way that the B band contains nearly all the intensity, while the Q band is weak. Comparing UV−vis spectra of $(NiL)_2$ and $(ZnL)_2$ with those of NiP and ZnP, one can notice that the strongest absorption bands located at 517.5 nm (2.40 eV) for $(NiL)_2$ and at 503.8 nm (2.46 eV) for $(ZnL)_2$ correspond

to the Q band of metal−porphyrin. Comparing the molecular symmetry of $(NiL)_2$ and $(ZnL)_2$ with that of NiP and ZnP, the symmetry-breaking changes the accidental degeneracy of the a_{1u} and a_{2u} orbitals significantly. This diminishes interaction between the $a_{1u}{}^1e_g{}^1$ and $a_{2u}{}^1e_g{}^1$ configuration and removes the forbidden character of the low-energy transition. Therefore, the Q band is no longer weak in $(NiL)_2$ and $(ZnL)_2$. The broad weak band located at 370.1 nm (3.35 eV) for $(NiL)_2$ and 351.7 nm (3.53 eV) for $(ZnL)_2$ can correspond to the very strong B band of metal−porphyrin. Furthermore, we find that local conjugation makes the absorption wavelength of $(NiL)_2$ and $(ZnL)_2$ shift to blue compared with those of NiP and ZnP.

Conclusions

The ground-state geometry, electronic structure, vibrational spectra, and electronic absorption spectra of $(ZnL)_2$ and $(NiL)_2$ [L = bis(2,4-dimethyldipyrrin-3-yl)methane] have been studied by DFT and TD-DFT methods employing the B3LYP hybrid functional and various basis set combinations. An enlarged basis set improves calculated bond lengths but gives a negligible alteration of the bond angles. The calculated vibrational wavenumbers are in good agreement with the experimental fundamentals with the deviations generally less than 30 cm^{-1}. In comparison of spectra with those of metal−porphyrin, the breathing vibration of the pyrrole ring is shifted by 100 cm^{-1} toward higher wavenumber due to local electronic conjugation. The TD-DFT method provides a good description of excitation energy. Because of the symmetry-breaking, the absorption bands (corresponding to the Q band of porphyrin) of $(ZnL)_2$ and $(NiL)_2$ are no longer weak. Local conjugation makes the absorption wavelength of $(NiL)_2$ and $(ZnL)_2$ shift to the blue compared with those of NiP and ZnP.

Acknowledgment. Financial support from the National Natural Science Foundation of China, Foundation of Wuhan University of Science and Engineering, and the Deutsche Forschungsgemeinschaft is highly acknowledged (contract/grant sponsors: Foundation of Wuhan University of Science and Engineering, Contract/Grant No. 20063103; National Natural Science Foundation of China, Contract/Grant Nos. 20375029, 2427002, and 20405011; Deutsche Forschungsgemeinschaft Grant Nos.446 CHV-112/52/02 and 446 CHV-112/12/04). W.K. and A.S. thank the Founds der Chemischen Industrie for financial support.

References and Notes

(1) Mitra, D.; Di Cesare, N.; Sleiman, H. F. *Angew. Chem., Int. Ed.* **2004**, *43*, 5804.
(2) Liang, K.; Zheng, H. G.; Song, Y. L.; Lappert, M. E.; Li, Y. Z.; Xin, X. Q.; Huang, Z. X.; Chen, J. T.; Lu, S. F. *Angew. Chem., Int. Ed.* **2004**, *43*, 5776.
(3) Papaefstathiou, G. S.; Zhong, Z. M.; Geng, L.; MacGillivray, L. R. *J. Am. Chem. Soc.* **2004**, *126*, 9158.
(4) Halper, S. R.; Cohen, S. M. *Angew. Chem., Int. Ed.* **2004**, *43*, 2385.
(5) Yang, L. Y.; Zhang, Y.; Yang, G. Q.; Chen, Q. Q.; Ma, J. S. *Dyes Pigm.* **2004**, *62*, 27.
(6) Shang, X. F.; Yang, L. Y.; Li, W.; Chen Q. Q. ; Wang, Z. P.; Hu, J. M.; Ma, J. S. *J. Chem. Crystallogr.* **2004**, *34*, 433.
(7) Zhang, Y.; Wang, Z.; Yan, C.; Li, G.; Ma, J. *Tetrahedron Lett.* **2000**, *41*, 7717.
(8) Piguet, C.; Bernardinelli, G.; Hopfgartner, G. *Chem. Rev.* **1997**, *97*, 2005.
(9) Weissbuch, I.; Cohen, S.; Cohen, H.; Leiserowitz, L.; Lahav, M.; Kjaer, K.; Howes, P. B.; Als-Nielsen, J.; Lehn, J. M.; Baxter, P. N. W.; Hanan, G., S.; Schubert, U. S. *J. Am. Chem. Soc.* **1998**, *120*, 4850.
(10) Fujita, M.; Su, S. Y.; Kusukawa, T.; Funaki, H.; Ogura, K.; Yamaguchi, K. *Angew. Chem., Int. Ed.* **1998**, *37*, 2082.
(11) Baxter, P. N.; Hanan, G. S.; Lehn, J. M. *Chem. Commun.* **1996**, *17*, 2019.
(12) Funeriu, D. P.; Lehn, J. M.; Baum, G.; Fenske, D. *Chem.−Eur. J.* **1997**, *3*, 99.
(13) Zhang, Y.; Thompson, A.; Rettig, S. J.; Dolphin, D. *J. Am. Chem. Soc.* **1998**, *120*, 13537.
(14) Chen, Q.; Zhang, Y.; Dolphin, D. *Tetrahedron Lett.* **2002**, *43*, 8413.
(15) Thompson, A.; Dolphin, D. *J. Org. Chem* **2000**, *65*, 7870.
(16) Thompson, A.; Rettig, S. J.; Dolphin, D. *Chem. Commun.* **1999**, 631.
(17) Falk, H. *The Chemistry of Linear Oligopyrroles and Bile Pigments;* Springer-Verlag: Wien, Austria, 1989.
(18) Dolphin, D. *The Porphyrins*; Academic Press: New York, 1979.
(19) Chen, Q.; Dolphin, D. *Can. J. Chem.* **2002**, *80*, 1668.
(20) Chen, Q.; Dolphin, D. *Tetrahedron Lett.* **2001**, *42*, 3263.
(21) Sazanovich, I. V.; Kirmaier, C.; Hindin, E.; Yu, L. H.; Bocian, D. F.; Lindsey, J. S.; Holten, D. *J. Am. Chem. Soc.* **2004**, *126*, 2664.
(22) Yu, L. H.; Muthukumaran, K.; Sazanovich, I. V.; Kirmaier, C.; Hindin, E.; Diers, J. R.; Boyle, P. D.; Bocian, D. F.; Holten, D.; Lindsey, J. S. *Inorg. Chem.* **2003**, *42*, 6629.
(23) D'Souza, F.; Smith, P. M.; Zandler, M. E.; McCarty, A. L.; Itou, M.; Araki, Y.; Ito, O. *J. Am. Chem. Soc.* **2004**,*126*, 7898.
(24) Pulay, P.; In *Applications of Electronic Structure Theory*; Schaefer, H. F., III., Ed.; Plenum: New York, 1977; p 153.
(25) Wong, M. W. *Chem. Phys. Lett.* **1996**, *256*, 391.
(26) Bytheway, I.; Wong, M. W. *Chem. Phys. Lett.* **1998**, *282*, 219.
(27) (a) Kozlowski, P. M.; Zgierski, M. Z.; Pulay, P *Chem. Phys. Lett.* **1995**, *247*, 379. (b) Kozlowski, P. M.; Jarzecki, A. A.; Pulay, P. *J. Phys. Chem.* **1996**, *100*, 7007. (c) Baker, J.; Kozlowski, P. M.; Jarzecki, A. A.; Pulay, P. *Theor. Chem. Acc.* **1997**, *97*, 59. (d) Nauyen, K. A., Day, P. N.; Pachter, R. *J. Chem. Phys.* **1999**, *110*, 9135.
(28) Nguyen, K. A.; Day, P. N.; Pachter, R. *J. Phys. Chem.* **1999**, *103*, 7378.
(29) (a) Becke, A. D. *J. Chem. Phys.* **1993**, *98*, 5648. (b) Becke, A. D. *Phys. Rev. A* **1988**, *38*, 3098. (c) Becke, A. D. *J. Chem. Phys.* **1993**, *98*, 1372. (d) Vosko, S.H.; Wilk, L.; Nusair, M. *Can. J. Phys.* **1980**, *58*, 1200. (e) Lee, C.; Yang, W.; Parr, P. G. *Phys. Rev. B* **1988**, *37*, 785.
(30) *Hyper Chem Pro 6.03*; Hypercube Inc.: Gainesville, FL, 2001.
(31) (a) Bauernschmitt, R.; Ahlrichs, R *Chem. Phys. Lett.* **1996**, *256*, 454. (b) Casida, M.; Jamorski, C.; Casida, K. C.; Salahub, D. R. *J. Chem. Phys.* **1998**, *108*, 4439. (c) Stratmann, R. E.; Scuseris, G. E.; Frisch, M. J. *Chem. Phys.* **1998**, *109*, 8218.
(32) Frisch, M. J.; et al. *Gaussian98*; Gaussian, Inc.: Pittsburgh, PA, 1998.
(33) (a) Zerner, M. C.; Correa de Mello, P.; Hehenberger, M. *Int. J. Quantum Chem.* **1982**, *21*, 251. (b) Thompson, M. A.; Zerner, M. C. *J. Am. Chem. Soc.* **1991**, *113*, 8210. (c) Hanson, L. K.; Fajer, J.; Thompson. M. A.; Zerner, M. C. *J. Am. Chem. Soc.* **1987**, *109*, 4728.
(34) O'Boyle, N. M.; Vos, J. G. *GaussSum.4.0*; Dublin City University: 2003. Available at http://gausssum.sourceforge.net.
(35) Anthony, P. S.; Leo, R. *J. Phys. Chem.* **1996**, *100*, 16502.
(36) (a) Li, X. Y.; Czernuszewicz, R. S.; Kincaid, J. R.; Su, Y. O.; Spiro, T. G. *J. Phys. Chem.* **1990**, *94*, 31.
(37) Li, X. Y.; Czernuszewicz, R. S.; Kincaid, J. R.; Su, Y. O.; Spiro, T. G. *J. Phys. Chem.* **1990**, *94*, 47.
(38) Jarzecki, A. A.; Kozlowski, P. M.; Pulay, P.; Ye, B. H.; Li, X. Y. *Spectrochim. Acta, Part A* **1997**, *53*, 1195.
(39) Jentzen, W.; Turowska-Tyrk, I.; Scheidt, W. R.; Shelnutt, J. A. *Inorg. Chem.* **1996**, *35*, 3559.
(40) Keegan, J. D.; Stolzenberg, E.; Lu, Y. C.; Linder, R. E.; Barth, G.; Moscowitz, A.; Bunnenberg, E.; Djerassi, C. *J. Am. Chem. Soc.* **1982**, *104*, 4305.
(41) Canters, G. W.; Jansen, G.; Noort, M.; van der Waals, J. H. *J. Phys. Chem.* **1976**, *80*, 2253.
(42) Sekino, H.; Kobayashi, H. *J. Chem. Phys.* **1987**, *86*, 5045.